Biofabrication

PAPER

A perfusable, vascularized kidney organoid-on-chip model

Katharina T Kroll[1,2,3], Kimberly A Homan[3], Sebastien G M Uzel[1,2], Mariana M Mata[1,2], Kayla J Wolf[1,2], Jonathan E Rubins[1,2] and Jennifer A Lewis[1,2,4,*]

[1] Harvard University, Paulson School of Engineering and Applied Sciences, Cambridge, MA, United States of America
[2] Wyss Institute for Biologically Inspired Engineering, Boston, MA, United States of America
[3] Complex *in vitro* Systems, Safety Assessment, Genentech Inc, South San Francisco, CA, United States of America
[4] Harvard Stem Cell Institute, Cambridge, MA, United States of America
[*] Author to whom any correspondence should be addressed.

E-mail: jalewis@seas.harvard.edu

RECEIVED
18 December 2023

REVISED
15 May 2024

ACCEPTED FOR PUBLICATION
21 June 2024

PUBLISHED
5 July 2024

Keywords: kidney organoids, kidney-on-chip model, perfusion, vascularization, anastomosis

Supplementary material for this article is available online

Abstract

The ability to controllably perfuse kidney organoids would better recapitulate the native tissue microenvironment for applications ranging from drug testing to therapeutic use. Here, we report a perfusable, vascularized kidney organoid on chip model composed of two individually addressable channels embedded in an extracellular matrix (ECM). The channels are respectively seeded with kidney organoids and human umbilical vein endothelial cells that form a confluent endothelium (macrovessel). During perfusion, endogenous endothelial cells present within the kidney organoids migrate through the ECM towards the macrovessel, where they form lumen-on-lumen anastomoses that are supported by stromal-like cells. Once micro-macrovessel integration is achieved, we introduced fluorescently labeled dextran of varying molecular weight and red blood cells into the macrovessel, which are transported through the microvascular network to the glomerular epithelia within the kidney organoids. Our approach for achieving controlled organoid perfusion opens new avenues for generating other perfused human tissues.

1. Introduction

The emergence of human organ-on-chip platforms and organoids is ushering in a paradigm shift for preclinical drug testing, brought to the forefront in part by the FDA Modernization Act 2.0 [1, 2]. During preclinical testing, nephrotoxicity currently leads to 2% of failures, yet this rises to roughly 19% in Phase III trials [3]. Hence, there has been considerable effort devoted to creating human kidney-on-chip models, including proximal tubules [4–6], glomeruli-on-chip [7, 8] and, most recently, kidney organoid-on-chip models [9–12]. Yet, each of these models lacks important physiological features, such as drug transporter expression [13, 14], multicellular and architectural complexity, or perfusable vasculature—all of which are present in native kidney tissue. Kidney organoids differentiated from human stem cells under static culture conditions do recapitulate the desired multicellular and architectural complexity. However, they often lack a robust endothelial progenitor cell population. When kidney organoids are seeded on an adherent extracellular matrix (ECM) and subjected to superfusive flow, pronounced microvessel formation with concomitant maturation of their glomerular and tubular compartments occurs [9]. However, these organoid microvessels are not capable of sustaining controlled perfusion. The ability to luminally perfuse these microvascular networks would enable delivery of new drug candidates, including immune cells, in a more physiologically relevant manner [12].

Unfortunately, to date, perfusable kidney organoids have only been achieved via transplantation subcutaneously [15], in the subcapsular region in mice [16, 17], or in the coelomic cavity of the chick embryo [18], where organoids are vascularized by invasion of host vessels. These *in vivo* approaches are not amenable to high throughput drug testing or therapeutic use. Efforts to achieve vascular

perfusion of kidney organoids *in vitro* have focused on organoids seeded on top of pre-engineered capillary beds [19] or individually patterned vessels [10] to mimic the 'outside (host)-in (organoid)' vascularization achieved *in vivo*. However, this strategy has not yet achieved success.

We posit that an ideal approach for *in vitro* vascularization of kidney organoids is to promote 'inside-(organoid microvessels)-out (patterned macrovessel)' anastomosis [16]. Here, we demonstrate the *in vitro* generation of an intravascular perfusable kidney organoid-on-chip model. Specifically, we create a millifluidic chip that contains two individually addressable channels embedded in a gelatin-fibrin matrix. Kidney organoids are seeded in one channel and are initially subjected to superfusive flow to enhance their endogenous endothelial progenitor cell population [9], while the other channel is seeded with human endothelial cells to create a bioengineered macrovessel [20]. We find that kidney organoid-derived microvessels migrate towards and anastomose with the bioengineered macrovessel. Once these luminal connections form, fluorescently labeled dextrans and red blood cells are introduced through the bioengineered macrovessel and subsequently perfuse through the kidney organoid-derived microvascular network. Through imaging, we show that these perfused species are present in capillaries adjacent to nephron epithelia within the kidney organoids. Our perfusable kidney organoid model offers a more physiologically relevant route for delivering both drug compounds and cells. Finally, the ability to create vascularized kidney tissue with hierarchical microvessel-macrovessel networks paves the way for organ-scale manufacturing via methods such as sacrificial writing in functional tissue [21, 22].

2. Materials and methods

2.1. Cell culture

H9 and GFP-H9 embryonic stem cells (ESCs) were purchased from WiCell and cultured on 1% growth factor reduced Matrigel (Corning) in mTeSR Plus stem cell culture medium (Stem Cell Technologies). Upon reaching confluence of ∼85%, the cells were split at a ratio of 1:20–1:25 (without centrifugation) using 5 μm ROCK inhibitor (Y-27 632 dihydrochloride, Tocris). The following day, ROCK inhibitor was removed from the culture. After thawing from cryostorage, the H9s were passaged at least 3 times before initiating kidney organoid differentiation to allow for cell line stabilization. All cell culture and organoid differentiation protocols were carried out in an incubator held at 37 °C, 95% humidity and 5% CO_2.

Human umbilical vein endothelial cells (HUVECs, pooled from multiple donors) were purchased from Lonza and cultured in endothelial growth medium 2 (EGM-2) at passage 2. Upon reaching ∼95% confluence, the cells were passaged using 0.25% trypsin (Gibco) and DMEM with 10% FBS as a quenching agent. The single cell solution obtained was counted using a Countess cell counter (Thermo Fisher) and the quenching agent was removed by centrifugation at 220× g and discarding of the supernatant. The cell pellet was reconstituted in EGM-2 at the desired cell concentration for seeding into the chip devices or splitting into new 2D culture at splitting ratios ranging between 1:5 and 1:12. HUVECs were not used past passage 7. Green fluorescent protein labeled human neonatal dermal fibroblasts (GFP-HNDF) were purchased from Angioproteomie and cultured according to manufacturer's instructions.

2.2. Kidney organoid differentiation

Kidney organoids are differentiated according to published protocols [23, 24]. In this study we derived kidney organoid from H9 ESCs and GFP-H9 ESCs. Briefly, H9 and GFP-H9 ESCs are dissociated using Gentle Cell Dissociation Reagent (Stem Cell Technologies), seeded at density of 18 000–20 000 cells cm^{-2} in a 6-well plate with 2 ml of medium per well in mTeSR Plus supplemented with 5 μm ROCK inhibitor (Tocris) and differentiated into nephron progenitor cells (NPCs), i.e., metanephric mesenchyme, via a three-step differentiation protocol using 8 μm CHIR (Tocris), 10 ng ml^{-1} Activin A (R&D Systems) and 10 ng ml^{-1} Fibroblast Growth Factor 9 (FGF9, R&D Systems) sequentially over 8 days of culture in the differentiation medium Advanced RPMI (AdvRPMI, Thermo Fisher Scientific) supplemented with 1X GlutaMax (Thermo Fisher Scientific). On day 8, the NPCs are dissociated into single cells using a 15 min incubation with AccuMax (Stem Cell Technologies), counted and seeded into AgreeWell800 6-well plates (Stem Cell Technologies) at an aggregate size of 15 000 cells/aggregate. The aggregation is performed in AdvRPMI with 1X GlutaMax, 10 ng ml^{-1} FGF9 and 3 μm CHIR. 24 h post aggregation (day 9), the culture medium is changed to AdvRPMI with 1X GlutaMax with 10 ng ml^{-1} FGF9 and the aggregates are cultured in this medium for 72 h until day 12 of differentiation. Since not all seeded NPCs participate in aggregate formation, we estimate that the final cell count per aggregate is ∼12 000 cells. By day 10/11, depending on the appearance of vesicular structures (similar to figure 3(c) of the original protocol paper [23]) in the aggregate, organoids are then seeded on a static ECM mimic (control) or into the top channel (which is embedded in a gelatin-fibrin matrix) in our dual-channel millifluidic chip.

2.3. Engineered ECM

The gelatin-fibrin ECM is prepared as previously described [9]. Briefly, we combined 10 mg mL^{-1} fibrinogen, 3 wt% gelatin, 2.5 mM $CaCl_2$ and 0.2 wt% transglutaminase and incubated at 37 °C for 15 min to improve optical clarity [4]. Note, in some cases,

green fluorescent protein labeled human neonatal dermal fibroblasts (GFP-HNDFs) are added to the ECM by mixing 1–10 M GFP-HNDFs/ml^{-1} with the ECM solution prior to incubation. Next, the ECM solution ± GFP-HNDFs is rapidly mixed with a thrombin (stock) solution prepared at a ratio of 250:1, resulting in a final thrombin concentration of 2 U ml^{-1}.

2.4. Perfusable Chips

We created a perfusable millifluidic device embedded in ECM (figures 1(a) and S1(a)). First, the gasket is 3D printed using a PDMS (SE1700, DOW Chemical) ink with a base to crosslinker ratio of 1:10. Prior to printing, the ink is mixed using a speed mixer (Flaktek). The ink is then printed onto a glass slide (75 × 50 mm) using a custom-designed, multimaterial 3D bioprinter equipped with four independently addressable printheads mounted onto a 3-axis, motion-controlled gantry with a build volume of 725 mm × 650 mm × 125 mm (AGB 10 000, Aerotech Inc., Pittsburgh, PA USA). The PDMS gasket is cured at 80 °C overnight and autoclaved with the other components of the perfusion system for sterilization. Components that cannot be sterilized by autoclaving are submerged in 70% ethanol and subsequently dried in a biosafety cabinet. Next, the PDMS gasket is equipped with the perfusion pins with two custom made 2.37 mm outer diameter (OD), 2.15 mm inner diameter (ID), 55 mm long pins (McMaster Carr) for the upper (kidney organoid) channel and 1.27 mm OD, 0.84 mm ID, 38 mm long pins (Nordson EFD) for the lower (macrovessel) channel (figure S1(b)). To generate open lumens within our ECM, two inner pins are pushed through the perfusion pins. The inner pin dimensions are 1.82 mm OD, 1.62 mm ID, length 120 mm for the kidney organoid channel and 0.71 mm OD, 0.51 mm ID, length 100 mm for the macrovessel. Once the inner pins are placed in the device, the pins are coated with a cotton applicator with 5% Pluronic-F127 (Sigma Aldrich) in water to avoid adherence of the ECM to the inner pins. The PDMS gasket is then filled with ECM solution and cured at 37 °C, 95% humidity and 5% CO2 for 3–4 h in a sterile container in an incubator. Post-curing, the container is held at 4 °C for 30 min to ease the pin removal process. The inner pins are carefully removed leaving behind a 1.8 mm diameter kidney organoid channel and a 0.7 mm diameter macrovessel channel surrounded by ECM. The perfusion pins are cleared of any remaining matrix by pulling a modest vacuum. The perfusion system is then assembled and connected to the perfusion pins of the PDMS gasket. There are two culture medium reservoirs (Nordson EFD) filled with the respective medium required for each channel. Advanced RPMI with 1X GlutaMax, 1% antibiotic/antimycotic solution (Gibco) and 1.5% fetal bovine serum is perfused through the top channel [9], which is seeded with kidney organoids, while EGM-2 is perfused through the macrovessel channel. Each medium reservoir is closed at the top using a lid with a 0.2 μm filter to allow for sterile gas equilibration and is connected to 2-stop perfusion tubing (PharMed BPT, 0.51 mm ID, orange-yellow) via a leur lock nozzle with a 0.2 μm sterile filter in line. The 2-stop tubing is mounted on an Ismatec peristaltic 8-roller pump and the perfusion pins are connected to the 2-stop tubing via a silicone tubing adaptor. The same silicone tubing is looped back into the reservoir with a 12.5 mm, 1.27 mm OD, 0.84 mm ID pin at the end inserted into an opening in the reservoir lid closing the fluid circuit. Both inlet and outlet tubing are equipped with tubing clamps to stop fluid flow during culture medium changes. The channels are filled with their respective culture medium to ensure there are no defects in the ECM that would lead to crosstalk between the channels. If the channels are intact and separated, the PDMS gasket with the ECM is encased with a custom stainless steel base frame on the bottom and a custom acrylic lid (4 mm thick) connected by four screws. The entire device is placed into the incubator and perfused at a volumetric flowrate of 50 μl min^{-1} until HUVECs and kidney organoids are seeded into their respective channels.

2.5. Endothelial cell seeding

HUVECs are prepared from 2D cell culture as a single cell solution at a concentration of 10–12 M cells ml^{-1} in EGM-2. The single cell solution is slowly pipetted from the outlet into the bottom (macrovessel) channel (200 μl per channel), the perfusion tubing is reconnected and clipped. Presence of HUVECs in the macrovessel channel is confirmed by microscopy and the chip is then placed into the incubator. After 30 min, the chip is rotated 180° around its long axis. This process is repeated again after an additional 3 h. After 7 h, perfusion is resumed at 3.74 μl min^{-1} overnight until the kidney organoids are seeded in the top channel on the following day.

2.6. Kidney organoid seeding and culture

After the macrovessel channel is seeded with HUVECs, the kidney organoid channel is seeded with kidney organoids at day 10/11 of their differentiation (figure S1(a)). For this, the clipped inlet and outlet tubing of the upper channel are disconnected. A blunt needle with the dimensions of the upper channel inner pin is used to pick up 150–200 kidney organoid aggregates, carefully inserted into the upper channel from the outlet and the kidney organoids are deposited in the center of the upper channel. The needle is removed slowly while pushing out fluid to maintain the position of the kidney organoids in the channel. The inlet and outlet tubing are re-connected to the perfusion pins ensuring that any remaining bubbles are pushed out at the outlet. Depending on the status of differentiation of the kidney organoids,

the culture medium in the upper kidney organoid channel is supplemented with 10 ng ml^{-1} FGF9. The top channel seeded with kidney organoids is left clipped for 30 min in the incubator until perfusion is resumed at 3.74 μl min^{-1} overnight. The next day, the sterile filters in the fluid lines are removed and the flowrate is ramped up to 250 μl min^{-1} to reach similar fluid shear in the kidney organoid channel as used previously [9]. The resulting shear calculated via the Hagen-Poiseuille equation [25]:

$$\tau = \frac{32\,\mu Q}{\pi\, d^3} \quad (1)$$

where Q denotes the volumetric flowrate, μ denotes the dynamic viscosity of the culture medium (0.0008 Pa·s [26]) and d denotes the vessel diameter. Assuming that each channel is a straight cylinder with inelastic walls and that the cell culture media are Newtonian fluids, we calculate estimated shear stress values (at the walls) for the kidney organoid and macrovessel channels of 0.0581 dyn cm^{-2} and 0.987 dyn cm^{-2}, respectively.

Brightfield microscopy is used to track cellular migration from the seeded kidney organoids (top channel) to the macrovessel (bottom channel). Once the migrating cells reach the macrovessel, 1 mg ml^{-1} aminocaproic acid (ACA) is added to the culture medium perfused through the top channel with every subsequent medium change to inhibit matrix degradation (day 5–7 of perfusion). To fix the tissue for imaging, each chip is carefully opened with the lines unclipped and at level with the chip. The pins are removed, the tissue is placed in a container with 10% formalin (∼4% buffered paraformaldehyde, Sigma Aldrich) and fixed for 45 min at room temperature. Subsequently, the tissue is washed three times for 2 h in phosphate buffered saline with calcium and magnesium (PBS^{++}) and stored at 4 °C prior to immunostaining.

2.7. Barrier function assay

To assess macrovessel permeability, the chips are prepared as described above and perfused for 5 d. The culture medium in the top (kidney organoid) channel is supplemented with 1 mg ml^{-1} ACA on day 1 of perfusion to inhibit cellular migration to the macrovessel for this assay (i.e. to prevent micro-macrovessel anastomosis). This was done to ensure analysis of barrier function of the macrovessel in the presence of kidney organoids, but without the presence of stromal cells around the macrovessel. Fixable, fluorescently labeled dextrans of varying molecular weight are added to the culture medium in the macrovessel channel. The chips are then perfused for 5, 10, 15, 30 and 60 min. Three dextrans (supplementary table 1) are used: FITC-labeled 2 M Da dextran at 1 mg ml^{-1}, tetramethyl rhodamine-labeled 70 kDa dextran at 10 mg ml^{-1} and Alexa Fluor 647-labeled 10 kDa dextran at 10 mg ml^{-1} [17], which are anionic and lysine-fixable via formaldehyde fixation. In control chips, macrovessels are denuded of the endothelial lining by perfusion of 0.1% Triton-X in PBS^{++} for 5 min, as confirmed by brightfield microscopy. After the requisite perfusion time, the chips are fixed as described above. After washing out the fixative, the perfusable organoid chips are cut into 1 mm thick sections and imaged with a Leica laser scanning upright confocal microscope for qualitative assessment of dextran permeability (figure S1(c)).

2.8. Imaging and image analysis techniques

To visualize different cell types, morphology and localization, the fixed tissues are cut in 1 mm thick sections and immunostained. First, the sections are permeabilized and blocked in 2% donkey serum (Sigma) and 0.125% Triton-X100 (Sigma) in PBS^{++} overnight at 4 °C. Primary antibodies (supplementary table 1) are incubated for 3 d at 4 °C in staining solution (0.125% Triton-X100 and 1% bovine serum albumin (Sigma) in PBS^{++}) and washed out over the course of 8 h with three exchanges of PBS^{++}. Secondary antibodies raised in donkey are incubated overnight at 4 °C in staining solution. Nuclear counterstain is achieved by incubating the samples with 1 μg ml^{-1} 4′,6-Diamidine-2′-phenylindole dihydrochloride (DAPI) in staining solution for 1 h. Secondary antibodies and DAPI are washed out over the course of 8 h with three exchanges of PBS^{++}. The samples are imaged on a laser scanning confocal microscope (Zeiss) and processed in Fiji for maximum intensity projections and Imaris (Bitplane) for 3D reconstruction and rendering.

To quantify cell migration speed, brightfield microscopy images of chips seeded with kidney organoids in the top channel with or without endothelial cells in the lower channel are taken every 48 h. During these experiments, the bottom (macrovessel) channel is perfused with the same medium as the top (kidney organoid) channel (Adv RPMI), Adv RPMI supplemented with 10 ng ml^{-1} vascular endothelial growth factor A (VEGF, R&D Systems), EGM-2, or EGM-2 with 10 ng ml^{-1} VEGF. Note, when the bottom channel is perfused with Adv RPMI as a base medium, it does not contain endothelial cells, since they do not survive in this medium condition. To determine the effects of matrix degradation, the kidney organoid channel is supplemented with 1 mg ml^{-1} ACA. Using FIJI software, the distance between the two channels is measured, the edge of the migrating cell front is determined, and its distance to the macrovessel is recorded (figures S1(d) and S2(a)). The absolute value of the slope of a linear regression of the cell migration observed per chip is provided in units of μm/day (figure S2(a)).

To analyze microvascular network morphology, cross-sectional confocal microscopy images are taken and divided into kidney organoid microvessels as well

as microvessels in the ECM (figure S3(a)). Images acquired on both sections are subjected to Angiotool analysis [27]. The data is collected and analyzed in GraphPad Prism. Information about biological and technical replicates can be found in supplementary table 3.

2.9. RNA isolation

For RNA isolation, the RNeasy Plus Mini Kit (Qiagen) is used. To isolate RNA out of the kidney organoids and endothelial cells cultured under flow and static conditions, the samples and controls are harvested on day 1, 4, 7 and 10 after seeding. For the samples cultured on chip, the surrounding ECM is removed with a scalpel to the extent possible without damaging the tissue. The tissue is cut into two sections; one section contains the kidney organoids and microvessels in the ECM, while the other section contains the macrovessel and surrounding cells associated with microvessels that have migrated from the organoids. Each tissue section is subsequently placed in 600 μl lysis buffer supplied in the Qiagen kit and vortexed until the tissue is dissolved. The samples are frozen in lysis buffer at −80 °C until RNA extraction is performed according to the manufacturer's instruction. RNA is eluted in 60 μl of RNAse-free water and RNA concentration and purity is analzed on a Nanodrop^{TM} Spectrophotometer (Thermo Scientific).

2.10. Nanostring gene expression analysis

Gene expression is analyzed by Nanostring nCounter analysis. A set of custom probes was selected to cover expression of kidney specific genes, endothelial cell specific genes and matrix processing genes along with housekeeping genes. Data analysis is performed in the nSolver (Nanostring) to normalize the counts of each individual gene to the housekeeping genes (GAPDH, ACTB, TUBB, PABPN1, YWHAZ, PPIA). Subsequently, samples collected from section 1 (containing kidney organoids and microvessels, see figure 2(a)) are normalized to static controls grown on the same ECM, but without flow stimulation, collected on the day corresponding to day 7 of perfusion. Samples collected from section 2 (containing macrovessel, microvessels and stromal/pericyte like cells, see figure 2(a)) are normalized to the sample collected of section 2 at day 1. A full list of genes can be found in supplementary table 2.

2.11. Perfusion assays

To assess the kidney organoid-derived microvasculature, a perfusion assay is performed after 10–12 d on chip. The bottom (macrovessel) channel is perfused with cell culture medium supplemented with either 1 mg ml^{-1} of FITC-labeled 2 M Da lysine fixable dextran or with 1 mg ml^{-1} of FITC-labeled 2 M Da lysine fixable dextran and 10 mg ml^{-1} of tetramethyl rhodamine-labeled 70 kDa lysine fixable dextran. The fluid reservoir that feeds the macrovessel channel is raised ∼13 cm above the kidney organoid channel leading to a pressure difference between the two channels of ∼130 mm H_2O or ∼9.6 mm Hg. The chip is then perfused at 250 μl min^{-1} for both channels for 24 h and subsequently fixed. The samples are then cut into 1 mm thick sections, counterstained for markers of interest and imaged by confocal microscopy.

To further assess the kidney organoid-derived microvasculature, a second perfusion assay is carried out using washed red blood cells (Innovative Research) after 10–12 d of chip. First, 5 ml of cell culture medium is supplemented with 1 ml of red blood cell solution leading to a hematocrit ∼ 5% red blood cells (settled by gravity). The fluid reservoir feeding the bottom (macrovessel) channel is raised ∼ 13 cm above the kidney organoid channel leading to a pressure difference between the two channels of ∼130 mm H_2O or ∼9.6 mm Hg. The chip is then perfused at 250 μl min^{-1} for both channels for 16 h and subsequently fixed. Then, the samples are cut into 1 mm thick sections, stained for markers of interest and imaged by confocal microscopy.

2.12. Statistical analysis

All bar graphs and dot plots are expressed as mean ± standard deviation. A detailed summary of biological and technical replicates, as well as kidney organoid batches used in each analysis can be found in supplementary table 3. Statistical analysis is done in GraphPad Prism and differences between samples were considered statistically significant with a p-value below 0.05 when running a one-way ANOVA with Tukey's post-test for multiple comparisons.

3. Results and discussion

The first step in generating perfusable kidney organoids on chip (figures 1(a), S1(a) and (b)) is to seed the macrovessel with endothelial cells. Using confocal microscopy coupled with immunofluorescent (IF) staining, we confirmed that a confluent endothelium forms within the embedded macrovessel in 2 d post seeding (figure 1(b)). Next, we introduce kidney organoids (day 10/11 of their differentiation) into the top channel, where they first adhere to the gelatin-fibrin matrix under static conditions prior to increasing culture medium flow (resulting in an estimated shear stress of 0.0581 dyn cm^{-2}). As expected, the kidney organoids fuse together and develop a pervasive endogenous microvessel network under these conditions (figures 1(c) and S1(c)) [9]. To evaluate barrier properties of the macrovessel, we carried out a qualitative permeability measurement using fluorescently labeled dextrans of varying molecular weight (figures 1(d) and S1(c)), which are perfused through macrovessels without and with confluent endothelium (± Endos). In the bare channel (− Endos, control), all dextran species rapidly diffuse into the surrounding gelatin-fibrin matrix

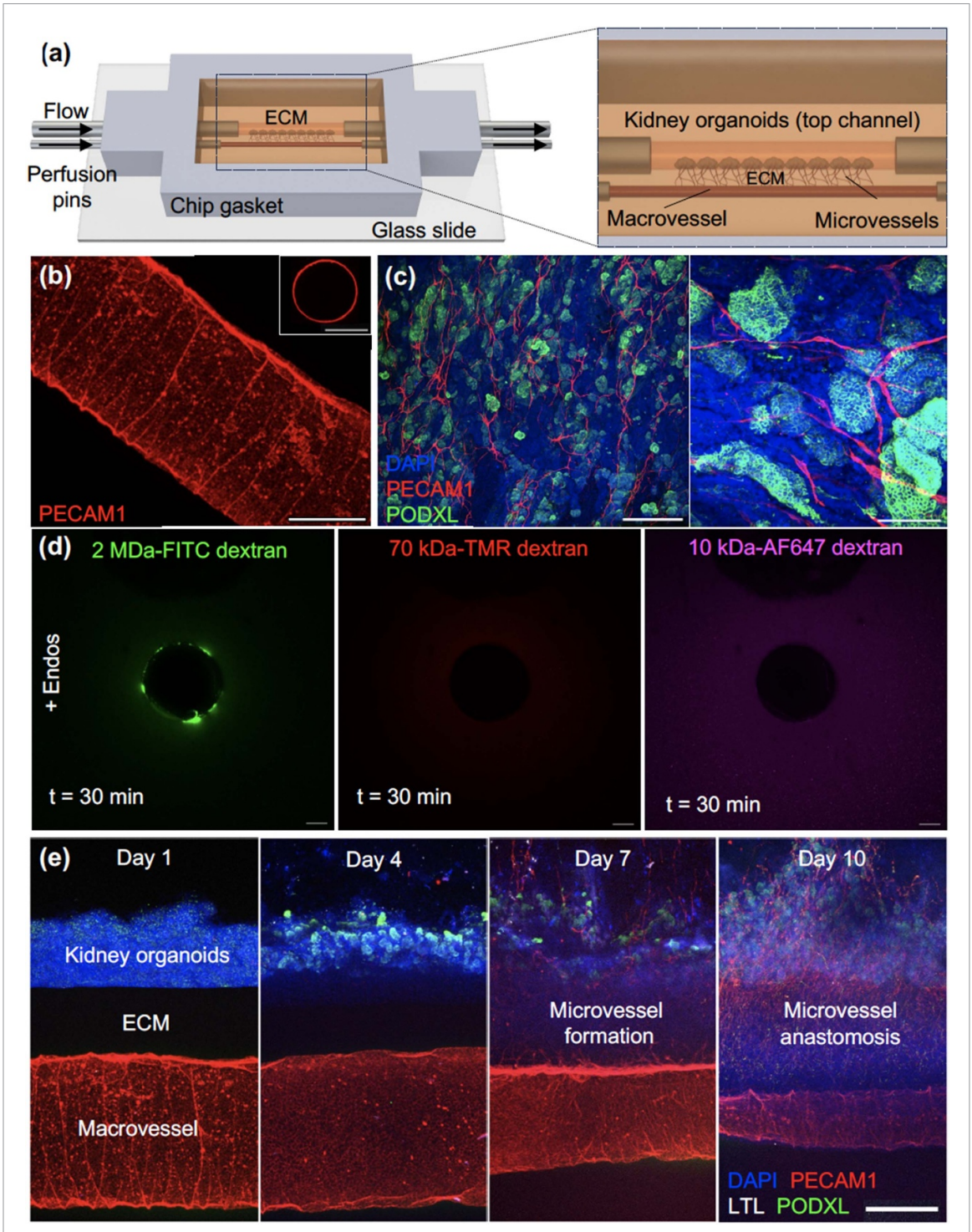

Figure 1. Perfusable kidney organoid-on-chip model. (a) Schematic illustration of the perfusable kidney organoid-on-chip model, in which endothelial cells are seeded in the bottom channel yielding a macrovessel and kidney organoids are seeded in the top channel on day 11/12 of their differentiation and then cultured under flow for 1–10 d. (b) Maximum intensity projection of representative confocal microscopy images of the macrovessel seeded with human umbilical vein endothelial cells (HUVECs) stained for PECAM1/CD31 (red), which show the resulting confluent endothelium in side-on and cross-sectional views (inset). (Scale bars are 500 μm.) (c) Representative maximum intensity projections of confocal microscopy images in low (left) and high (right) magnification (top-down views, day 5)) of the kidney organoids seeded and subjected to superfusive flow in the top channel, stained for nuclei (DAPI, blue), endothelial cells (PECAM1/CD31, red) and podocyte clusters (PODXL, green). (Scale bars are 500 μm, left and 100 μm, right). (d) Representative maximum intensity projections of cross-sectional confocal microscopy images of the macrovessel cultured for 5 d perfused with fixable fluorophore-conjugated dextrans of varying molecular weights acquired after 30 min of perfusion. (Scale bars are 200 μm.) (e) Representative maximum intensity projections of confocal microscopy images (side-view) of this perfusable kidney organoid-on-chip model on days 1, 4, 7 and 10 of flow, which is stained for nuclei (DAPI, blue), endothelial (PECAM1/CD31, red), proximal tubule epithelial (LTL, grey) and podocyte (PODXL, green) cells. (Scale bar is 500 μm).

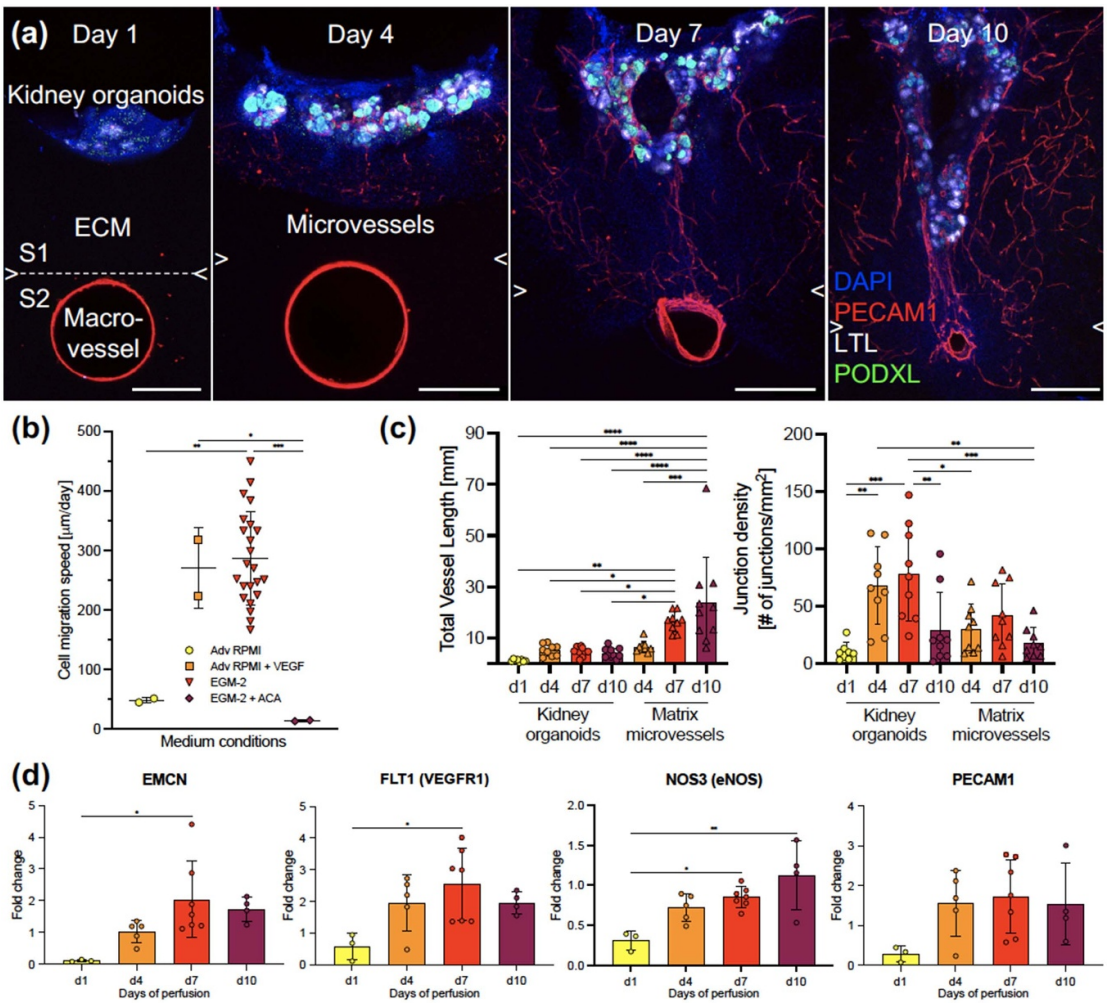

Figure 2. Microvessel network evolution. (a) Representative maximum intensity projections of confocal microscopy images (cross-sectional view) of the perfusable kidney organoid-on-chip model on days 1, 4, 7 and 10 of flow, stained for nuclei (DAPI, blue), endothelial (PECAM1/CD31, red), proximal tubule epithelial (LTL, grey) and podocyte (PODXL, green) cells. The dashed line in the day 1 image indicates the cut between the two sections for RNA isolation, where section 1 (S1) contains predominantly kidney organoids and migrating microvessels embedded in matrix and section 2 (S2) contains the macrovessel and adjacent microvessels. The cut locations are also indicated by the notches at the edges of the day 4 to day 10 images. (Scale bar is 500 μm). (b) Plot of the cell migration velocity as a function of media composition perfused through the macrovessel. Four media compositions were evaluated: Advanced RPMI (Adv RPMI) with or without 10 ng ml^{-1} vascular endothelial growth factor (VEGF) and endothelial growth medium 2 (EGM-2) which contains 2 ng ml^{-1} vascular endothelial growth factor with or without 1 mg ml^{-1} aminocaproic acid. (c) Angiotool analysis of microvessels present within the kidney organoids and matrix between the two channels. (d) Nanostring gene expression analysis of section 1, which is composed of kidney organoids and microvessels in the matrix on day 1, day 4, day 7 and day 10 of flow on chip. All gene expression is normalized to static conditions equivalent to day 7 of flow. Asterisks indicate p-values in the one-way ANOVA with Tukey's post-test as follows: $^{*}p < 0.0332$, $^{**}p < 0.0021$, $^{***}p < 0.0002$, $^{****}p < 0.0001$.

(figure S1(c)). However, in the presence of a confluent endothelium, the larger dextran (70 kDa and 2 M Da) species remain within the macrovessel lumen, where the 2 M Da dextran species are uptaken by endothelial cells (figure 1(d)). Only the smallest dextran (10 kDa) species perfused through the endothelialized macrovessel are able to diffuse into the surrounding gelbrin matrix indicating that the engineered macrovessels exhibit barrier function.

To promote micro-macrovessel integration, we perfuse the kidney organoid-on-chip models for up to 14 d. During this period, significant cell migration occurs from the kidney organoids (top channel) through the matrix to the endothelialized macrovessel (bottom channel) (figures 1(e), S1(d) and 2(a)). The cell migration speed depends on the composition of the culture medium perfused through the macrovessel (figures 2(b) and S2(a)). Interestingly, few cells migrated towards the macrovessel when the organoid-seeded and macrovessel channels are perfused with the same culture medium (Adv RPMI). However, upon adding VEGF to this medium in the bottom channel, the cell migration speed drastically increases, i.e., migrating cells appear to respond to the VEGF gradient that arises between the organoid-seeded and macrovessel channels (figures 2(b) and S2(a)). Additionally, when matrix degradation is inhibited by the addition of ACA [28] in the medium perfused through the top (kidney organoid) channel, cell migration is halted. Cell migration is therefore

coupled with their ability to locally degrade or alter the matrix both resides between and surrounding the two embedded channels.

To determine the migrating cell composition, we stained tissue cross-sections for the endothelial marker PECAM1 (CD31), glomerular marker podocalyxin (PODXL) and proximal tubule marker LTL to visualize endothelial, podocyte-rich glomeruli, and proximal tubules, respectively, at different timepoints (figures 2(a) and S2(b)). At day 1 after organoid seeding, we confirmed the presence of the confluent endothelium in the macrovessel by CD31 staining as well as adherent kidney organoids (top channel). At this early time point, the glomerular and tubular features are not yet fully formed. After 4 d of perfusion, one can readily observe such features, as denoted by their respective cell markers. Concomitantly, we also clearly observe the migrating cell front ($DAPI^+$ cells). Interestingly, by day 4, microvessel networks composed of endogenous endothelial cells ($CD31^+$) have formed around both podocyte ($PODXL^+$) clusters and proximal (LTL^+) tubules. Endogenous endothelial ($CD31^+$) cells are also present at the migrating cell front within the matrix between channels, where both individual cells and more chord-like structures are observed [29, 30]. At day 7 of perfusion, the migrating cell front reaches the macrovessel (bottom channel), while kidney organoids remain within the top channel. We do not observe preferential association of the microvasculature with either glomerular or tubular features (figure S2(c)). By day 10 of perfusion, the kidney organoids have further degraded the matrix allowing them to migrate towards the macrovesel. Importantly, we also find that organoid-derived microvessels form lumen-on-lumen connections to the macrovessel via processes that, in some cases, involve angiogenic sprouting from macrovessel towards to migrating microvessels. We find that the luminal diameter of the macrovessel also decreases over this 10 d period, likely due to ECM degradation. While the macrovessel remains patent, this results in an increased luminal shear stress of $\sim$20 dyn cm^{-2}, which remains within physiological range [25].

To assess the morphology of the microvessel network in the kidney organoids compared to those that migrate within the matrix, we performed Angiotool analysis of distinct tissue sections on chip (figures 2(c) and S3(a)). While the total vessel length of microvessels within the kidney organoids remains nearly the same during days 4–10 of perfusion, we observe a pronounced increase in microvessel length for the migrating network. We also observe that the junction density decreases in both microvessel networks, i.e., those present within the kidney organoids and the matrix, which is likely indicative of microvessel remodeling [31]. To further characterize these networks, we carried out Nanostring gene expression analysis of these two tissue sections (figure 2(a)), in which section 1 predominantly contains kidney organoids and the migrating microvessel network in the matrix, while section 2 contains the macrovessel and adjacent microvessels. We find that vascular markers, such as endoglin (ENG), endomucin (EMCN), VEGF receptor 1 (FLT1), endothelial nitric oxide synthase (NOS3), PECAM1 ($CD31^+$), nuclear receptor subfamily 2, group F, member 2 (NR2F2), Tyrosine kinase with immunoglobulin-like and EGF-like domains 1 (TIE1), and Cell division control protein 42 homolog (CDC42), are increasingly expressed putatively within the microvessels that reside in both the kidney organoids and surrounding matrix. The upregulation of these key markers is reflective of vascular cells undergoing angiogenesis (figures 2(d) and S3(b)) [32–34]. Interestingly, expression of apelin receptor 1, thrombomodulin, VEGF A, and von Willebrandt factor (vWF), in addition to EMCN, FLT1, NOS3, and PECAM1 ($CD31^+$) are also detected in the second tissue section 2 containing the macrovessel and adjacent microvessels (figure S3(c)). Hence, over time, there is an increased presence of vascular cells in this region. In addition to vascular markers, we investigated the expression of renal markers (figure S3(d)).

To determine the identity of migrating cells that are $CD31^-UEAI^-$, we stained the tissue cross-sections for vascular (UEAI), pericyte-like and mesenchymal cell markers, including PDGFRb, COL1A1, actin and ACTA2, and the renal stromal cell marker, homeobox protein Meis1 and 2, MEIS 1 and MEIS2 (figures 3(a), S4(a) and (b)), supplementary videos 1-3) [35, 36]. Notably, $CD31^-$ migrating cells closely associated with the migrating microvessel network and macrovessel are positive for MEIS1, PDGFRb, and ACTA (figures 3(a), S4(a) and (b)), supplementary videos 1−3). We then carried out Nanostring gene expression analysis of pericyte and stromal cell related genes as well as matrix deposition and remodeling (figures 3(b), (c) and S4(c)−(e)) in these same two tissue sections. In section 1, kidney organoids, ECM microvessels and accompanying cells, markers for both renal, MEIS1/2, and other stromal cells (α smooth muscle actin, ACTA2; angiopoetin 1, ANGPT1; insulin-like growth factor 1, IGF1; platelet-derived growth factor receptor beta, PDGFRb; vimentin, VIM) and pericytes (chondroitin sulfate proteoglycan 4, CSPG4 (NG2); desmin—DES; regulator of G-protein signaling 5, RGS5) exhibit increased expression over this same 10 d time (figures 3(b) and S4(c)). Given their close association with microvessels, we infer that such cells not only support cell migration, but serve as mural cells for migrating vasculature. We also find that cells

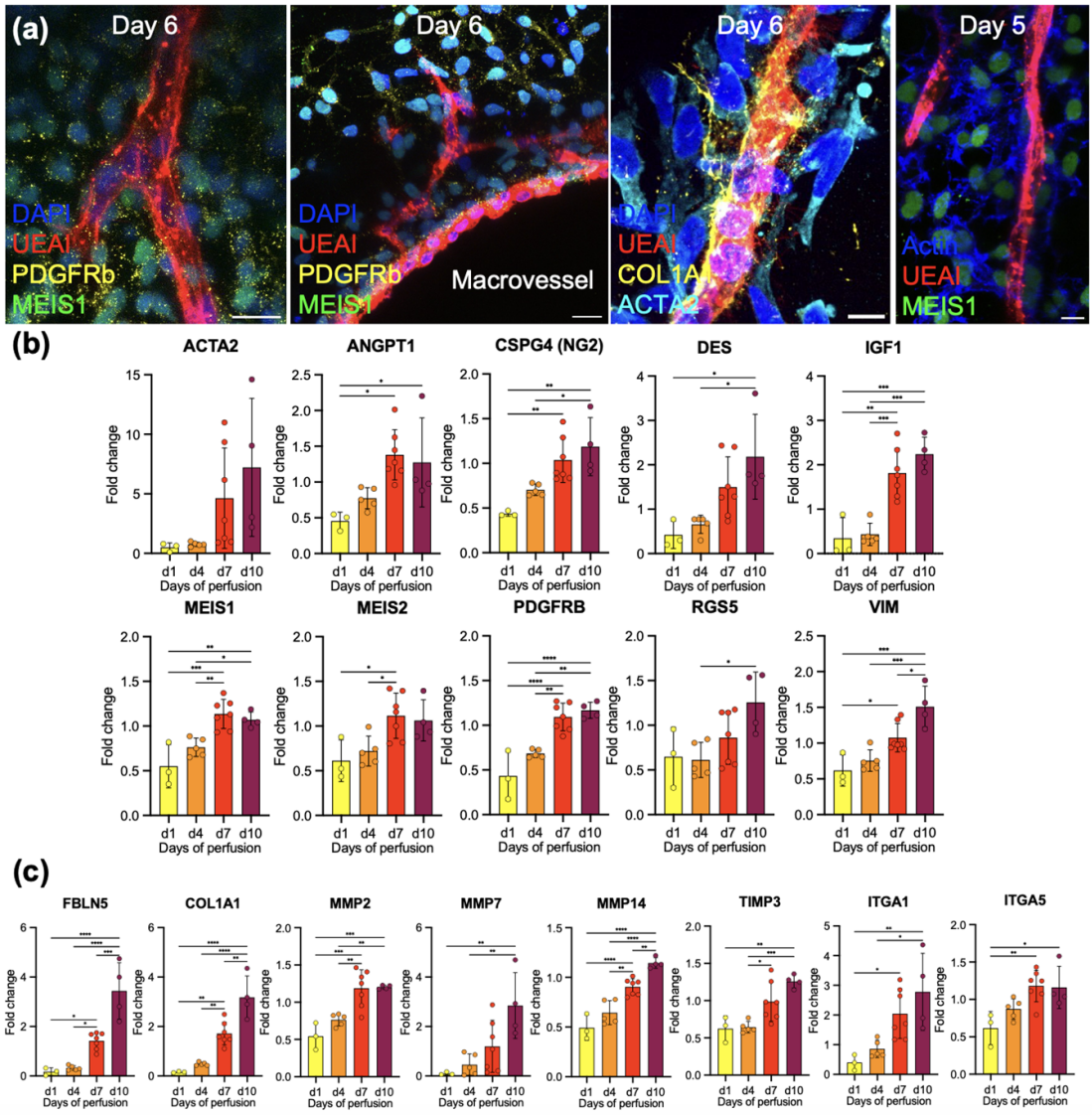

Figure 3. Stromal cell distribution. (a) Representative maximum intensity projections of confocal microscopy images (cross-sectional view) of the perfusable kidney organoid-on-chip model on day 5 and 6 of flow, stained for nuclei or actin (DAPI, Actin, blue), endothelial cells (UEAI, red), and stromal and pericyte markers (MEIS 1, green, PDGFRb, COL1A1, yellow and ACTA2, cyan). The images are acquired for representative microvessels in the matrix or adjacent to the macrovessel. (Scale bars are 20 μm, left two images and 10 μm, right two images). (b, c) Nanostring gene expression analysis of section 1, which is composed of kidney organoids and microvessels in the matrix on day 1, day 4, day 7 and day 10 of flow on chip. All gene expression is normalized to static conditions equivalent to day 7 of perfusion. Asterisks indicate p-values in the one-way ANOVA with Tukey's post-test as follows: $^{*}p < 0.0332$, $^{**}p < 0.0021$, $^{***}p < 0.0002$, $^{****}p < 0.0001$.

with ACTA2, DES, CSPG4, and PDGFRb markers are present on day 10 of perfusion in the tissue section 2, indicating that stromal/pericyte-like cells support the macrovessel and adjacent microvessels (figure S4(d)).

Not surprisingly, we observed increased expression of genes related to matrix deposition [37] (fibulin 5, FBLN5; collagen I, COL1A1) and matrix remodeling (matrix metalloproteinase-2, 7, 14, MMP2, MMP7, MMP14; tissue inhibitor of metalloproteinases 2, TIMP2) (figures 3(c), S4(d) and (e)) suggesting that active remodeling of the gelatin-fibrin matrix between the organoid- and endothelial-seeded channels is necessary for the observed migration of both endothelial and supporting cells (stromal cells and pericytes). Notably, MMP2 has been implicated in matrix remodeling during angiogenesis *in vivo* and *in vitro* [38]. These data are aligned with our observations that inhibiting matrix degradation halts cell migration (figure 2(b)). Integrins, like ITGA1 and ITGA5, are also upregulated, which are vital for cell interactions with the surrounding matrix (figure 3(c)) [37]. Taken together, our observations suggest that formation and maintenance of kidney organoid-derived microvessels rely on these supporting cell types to degrade the matrix and deposit their own basement membrane [39].

To assess micro-to-macrovessel anastomosis, we examined the potential luminal connection points of the microvasculature with the macrovessel by confocal microscopy (figures 4(a) and (b)). We

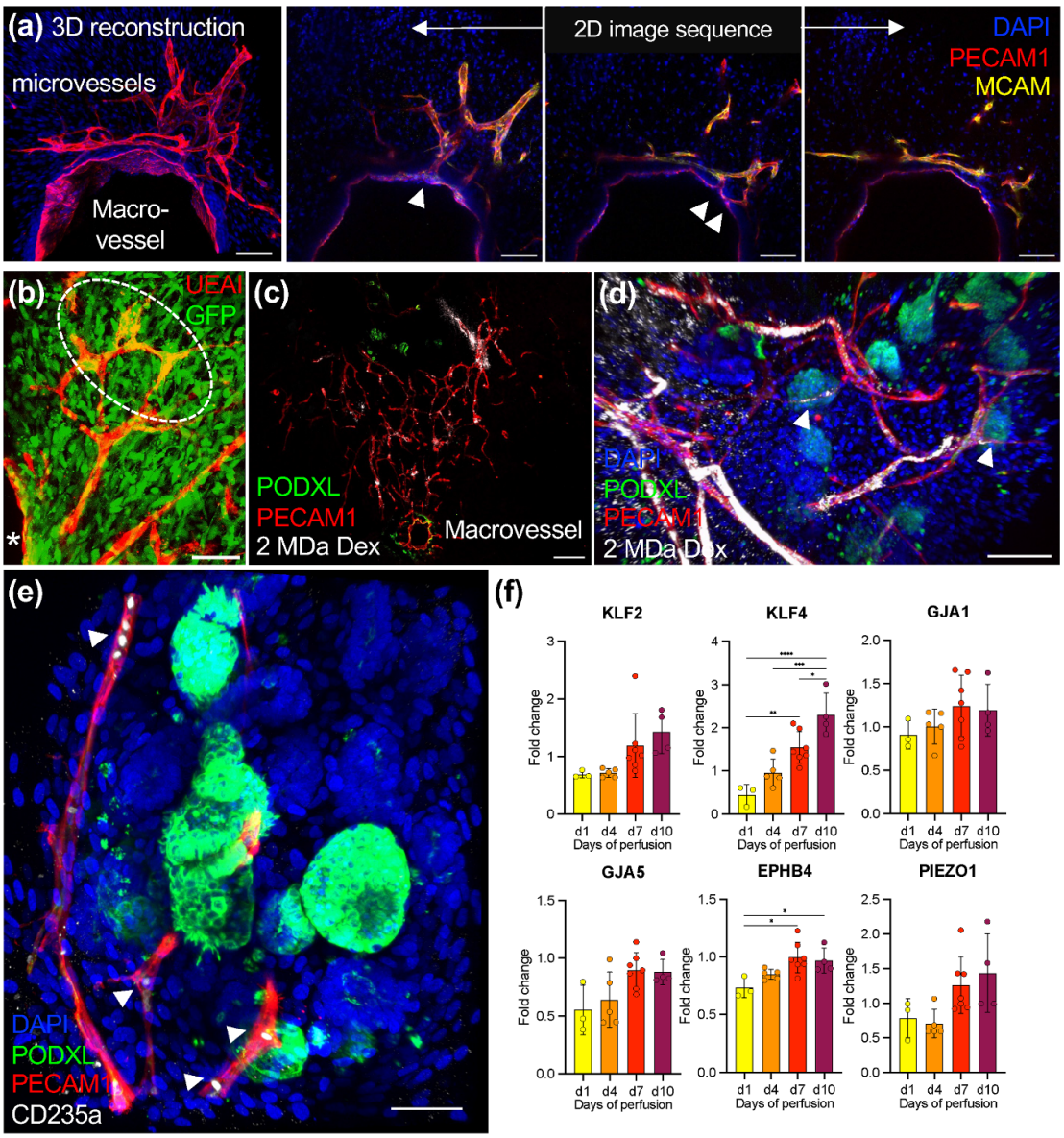

Figure 4. Microvascular anastomosis and perfusion. (a) 3D reconstruction (left) and z-stack confocal images (right) of the macrovessel after anastomosis (day 14 of perfusion) with kidney organoid-derived microvessels, stained for nuclei (DAPI, blue) and endothelial cells (PECAM1/CD31, red and MCAM, yellow). The white arrows highlight lumen-on-lumen anastomoses of microvessels to the macrovessel. (Scale bars are 100 μm). (b) Representative maximum intensity projection of confocal microscopy images (cross-sectional view) of the perfusable kidney organoid-on-chip model on day 7 where endothelial cells are stained for UEAI (red). Green fluorescent protein (GFP)-expressing kidney organoids enable one to distinguish between microvessels derived from kidney organoids (yellow) versus vascular sprouts that originate from the macrovessel (red). *Denotes the macrovessel and the dotted line encircles the GFP^+ to GFP^- connection in the $UEAI^+$ vasculature (Scale bar is 20 μm). (c), (d) Representative maximum intensity projection and 3D reconstruction, respectively, of confocal microscopy images (cross-sectional views) of the perfusable kidney organoid-on-chip model on day 10 of flow, stained for nuclei (DAPI, blue), endothelial (PECAM1/CD31, red) and podocyte cells (PODXL, green) after perfusing 1 mg ml^{-1} fluorescently labeled, fixable 2 M Da dextran (2 M Da Dex, grey) for 24 h under a pressure gradient of ~9.6 mm Hg between the macrovessel (higher pressure) and top channel seeded with kidney organoids (lower pressure). (Scale bars are 200 μm, left and 100 μm, right). (e) Representative 3D reconstruction of confocal microscopy image (cross-sectional view) of the perfusable kidney organoid-on-chip model on day 10 of flow, stained for nuclei (DAPI, blue), endothelial (PECAM1/CD31, red), podocyte (PODXL, green) and red blood cells (CD235a, grey). Red blood cells in the culture medium were perfused through the macrovessel for 16 h under a pressure gradient of ~9.6 mmHg between the macrovessel (higher pressure) and the top channel seeded with kidney organoids (lower pressure). (Scale bar is 50 μm). (f) Nanostring gene expression analysis of section 1, which is composed of kidney organoids and microvessels in the matrix on day 1, day 4, day 7 and day 10 of flow. All gene expression is normalized to static conditions equivalent to day 7 of perfusion. Asterisks indicate p-values in the one-way ANOVA with Tukey's post-test as follows: $^*p < 0.0332$, $^{**}p < 0.0021$, $^{***}p < 0.0002$, $^{****}p < 0.0001$.

directly visualized luminal connections between $MCAM^+CD31^+$ microvessels and the embedded macrovessel. Because migrating stromal-like cells likely also interact with the macrovessel, we used kidney organoids derived from a GFP-labeled ESC line (GFP-H9) to discern the origin of cells within interconnected vessels, i.e. whether they formed solely due to cell migration and anastomosis to the

macrovessel or whether capillary sprouting from the macrovessel plays a role (figures 4(b) and figures S4(f), supplementary video 4). These experiments reveal that GFP^+CD31^+ microvessels originating from the kidney organoids do connect with sprouting capillaries originating from the macrovessel (GFP^-CD31^+), in which capillary anastomosis occurs ~150 μm away from the macrovessel.

To demonstrate organoid-derived microvascular perfusion via integrated micro-macrovessels, we introduced a high molecular weight, fluorescently labeled dextran (FITC, 2 M Da) through the macrovessel and applied a pressure gradient of ~9.6 mmHg across the top and bottom channels for 24 h (figure 4(c), supplementary video 5). After perfusion, we assessed the distribution of dextran via confocal microscopy and counter stained for vascular (CD31) and podocyte (PODXL) markers (figure 4(d), supplementary video 6). We find direct evidence of dextran species within $CD31^+$ microvascular networks present in the matrix and kidney organoids. Indeed, these dextran species are found in microvessels adjacent to podocyte-rich ($PODXL^+$) clusters. There also appears to be minor leakage of the dextran into the tissue from the microvessels potentially due to their immaturity. As a final demonstation, we perfused red blood cells through macrovessel to these interconnected microvessel networks. Again, we find that $CD235a^+$ red blood cells are delivered through the $CD31^+$ microvascular networks and reside in capillaries near podocyte-rich ($PODXL^+$) clusters (figure 4(e), supplementary video 7). We then evaluated the presence of mechanosensing genes in tissue section 1 using Nanostring analysis [40–45]. We observed upregulation of Krüppel-like Factor 2 and 4 (KLF2, KLF4), as well as gap junction proteins (GJA1, GJA5), Ephrin B4 (EPHB4) and Piezo-Type Mechanosensitive Ion Channel Component 1 (PIEZO1) suggesting a distinct response to flow on chip.

4. Conclusions

In summary, we created a perfusable, vascularized kidney organoid-on-chip model. We show that endothelial and stromal-like cells migrate from the kidney organoids through the surrounding matrix to a bioengineered macrovessel, potentially in response to a chemoattractant gradient. The confluent endothelialized macrovessel exhibits barrier function and forms capillary anastomoses with the migrating microvessels supporting their perfusion. We then demonstrate that both dextran and red blood cells could be perfused from the macrovessel through the microvessel network to podocyte-rich clusters present within kidney organoids. Looking ahead, these perfusable kidney organoid-on-chip models offer promise for assessing drug candidates (including cell-based therapeutics) as well as vascular damage linked to kidney disease. Moreover, the ability to connect endogenous microvesses within kidney organoid building blocks to patterned macrovessels opens new avenues for the scalable fabrication of human kidney tissue for therapeutic repair.

Data availability statement

The G-code designed to print the gasket will be made available on github [46]. Other data that support the findings of this study are available upon request from the authors.

All data that support the findings of this study are included within the article (and any supplementary files).

Competing Financial Interests

Trestle Biotherapeutics, Inc. has licensed patents related to kidney tissue engineering from Harvard University. J A L is a member of the Scientific Advisory Boards of Trestle Biotherapeutics and Roche's Institute for Human Biology. K A H is currently employed by Genentech, but carried out this work as a postdoctoral researcher in the Lewis Lab at Harvard.

Acknowledgments

We thank Drs. Ryuji Morizane, Navin Gupta, Ken Hiratsuka, Iain Drummond and Ondine Cleaver for useful discussions. This work was supported by the NIDDK Re(Building) a Kidney Consortium (NIH UC2DK126023) and International Foundation of Ethical Research Graduate Student Fellowship (awarded to K T K).

ORCID iDs

Katharina T Kroll https://orcid.org/0000-0001-5707-9109
Kimberly A Homan https://orcid.org/0000-0001-6103-0498
Kayla J Wolf https://orcid.org/0000-0001-6990-0283
Jonathan E Rubins https://orcid.org/0000-0001-6830-3110
Jennifer A Lewis https://orcid.org/0000-0002-0280-2774

References

[1] Nuwer R 2022 US agency seeks to phase out animal testing *Nature* (https://doi.org/10.1038/d41586-022-03569-9)
[2] Stresser D M *et al* 2023 Towards in vitro models for reducing or replacing the use of animals in drug testing *Nat. Biomed. Eng.* 1–6
[3] Irvine A R, van Berlo D, Shekhani R and Masereeuw R 2021 A systematic review of in vitro models of drug-induced kidney injury *Curr. Opin. Toxicol.* **27** 18–26

[4] Homan K A, Kolesky D B, Skylar-Scott M A, Herrmann J, Obuobi H, Moisan A and Lewis J A 2016 Bioprinting of 3D convoluted renal proximal tubules on perfusable chips *Sci. Rep.* **6** 34845

[5] Jang K-J, Mehr A P, Hamilton G A, McPartlin L A, Chung S, Suh K-Y and Ingber D E 2013 Human kidney proximal tubule-on-a-chip for drug transport and nephrotoxicity assessment *Integr. Biol.* **5** 1119–29

[6] Lin N Y C, Homan K A, Robinson S S, Kolesky D B, Duarte N and Moisan A 2019 Renal reabsorption in 3D vascularized proximal tubule models *Proc. Natl Acad. Sci. USA* **116** 5399–404

[7] Musah S *et al* 2017 Mature induced-pluripotent-stem-cell-derived human podocytes reconstitute kidney glomerular-capillary-wall function on a chip *Nat. Biomed. Eng.* **1** 0069

[8] Petrosyan A, Cravedi P, Villani V, Angeletti A, Manrique J, Renieri A, De Filippo R E, Perin L and Da Sacco S 2019 A glomerulus-on-a-chip to recapitulate the human glomerular filtration barrier *Nat. Commun.* **10** 3656

[9] Homan K A *et al* 2019 Flow-enhanced vascularization and maturation of kidney organoids in vitro *Nat. Methods* **16** 255–62

[10] Menéndez A B C *et al* 2022 Creating a kidney organoid-vasculature interaction model using a novel organ-on-chip system *Sci. Rep.* **12** 20699

[11] Hiratsuka K, Miyoshi T, Kroll K T, Gupta N R, Todd Valerius M, Ferrante T, Yamashita M, Lewis J A and Morizane R 2022 Organoid-on-a-chip model of human ARPKD reveals mechanosensing pathomechanisms for drug discovery *Sci. Adv.* **8** eabq0866

[12] Kroll K T *et al* 2023 Immune-infiltrated kidney organoid-on-chip model for assessing T cell bispecific antibodies *Proc. Natl Acad. Sci.* **120** e2305322120

[13] Ingber D E 2022 Human organs-on-chips for disease modelling, drug development and personalized medicine *Nat. Rev. Genet.* **23** 467–91

[14] Soo J Y C, Jansen J, Masereeuw R and Little M H 2018 Advances in predictive in vitro models of drug-induced nephrotoxicity *Nat. Rev. Nephrol.* **14** 378–93

[15] Bantounas I *et al* 2018 Generation of functioning nephrons by implanting human pluripotent stem cell-derived kidney progenitors *Stem Cell Rep.* **10** 766–79

[16] van den Berg C W *et al* 2018 Renal subcapsular transplantation of PSC-derived kidney organoids induces neo-vasculogenesis and significant glomerular and tubular maturation *in vivo Stem Cell Rep.* **10** 751–65

[17] Van Den Berg C W, Koudijs A, Ritsma L and Rabelink T J 2020 *In vivo* assessment of size-selective glomerular sieving in transplanted human induced pluripotent stem cell-derived kidney organoids *J. Am. Soc. Nephrol.* **31** 921–9

[18] Koning M *et al* 2022 Vasculogenesis in kidney organoids upon transplantation *npj Regen. Med.* **7** 40

[19] Zhang S, Wan Z and Kamm R D 2021 Vascularized organoids on a chip: strategies for engineering organoids with functional vasculature *Lab Chip* **21** 473–88

[20] Kolesky D B, Homan K A, Skylar-Scott M A and Lewis J A 2016 Three-dimensional bioprinting of thick vascularized tissues *Proc. Natl Acad. Sci. USA* **113** 3179–84

[21] Skylar-Scott M A, Uzel S G M, Nam L L, Ahrens J H, Truby R L, Damaraju S and Lewis J A 2019 Biomanufacturing of organ-specific tissues with high cellular density and embedded vascular channels *Sci. Adv.* **5** eaaw2459

[22] Wolf K J, Weiss J D, Uzel S G M, Skylar-Scott M A and Lewis J A 2022 Biomanufacturing human tissues via organ building blocks *Cell Stem Cell* **29** 667–77

[23] Morizane R, Lam A Q, Freedman B S, Kishi S, Valerius M T and Bonventre J V 2015 Nephron organoids derived from human pluripotent stem cells model kidney development and injury *Nat. Biotechnol.* **33** 1193–200

[24] Morizane R and Bonventre J V 2017 Generation of nephron progenitor cells and kidney organoids from human pluripotent stem cells *Nat. Protocols* **12** 195–207

[25] Papaioannou T G and Stefanadis C 2005 Vascular wall shear stress: basic principles and methods *Hellenic J. Cardiol.* **46** 9–15

[26] Poon C 2022 Measuring the density and viscosity of culture media for optimized computational fluid dynamics analysis of *in vitro* devices *J. Mech. Behav. Biomed. Mater.* **126** 105024

[27] Zudaire E, Gambardella L, Kurcz C and Vermeren S 2011 A computational tool for quantitative analysis of vascular networks *PLoS One* **6** e27385

[28] Kaseer H and Sanghavi D 2022 Aminocaproic Acid *StatPearls*

[29] Coultas L, Chawengsaksophak K and Rossant J 2005 Endothelial cells and VEGF in vascular development *Nature* **438** 937–45

[30] Arnaoutova I and Kleinman H K 2010 *In vitro* angiogenesis: endothelial cell tube formation on gelled basement membrane extract *Nat. Protocols* **5** 628–35

[31] Korn C and Augustin H G 2015 Mechanisms of vessel pruning and regression *Dev. Cell* **34** 5–17

[32] Cleaver O and Melton D A 2003 Endothelial signaling during development *Nat. Med.* **9** 661–8

[33] Barry D M *et al* 2019 Molecular determinants of nephron vascular specialization in the kidney *Nat. Commun.* **10** 5705

[34] Trimm E and Red-Horse K 2023 Vascular endothelial cell development and diversity *Nat. Rev. Cardiol.* **20** 197–210

[35] Sims D E 2000 Diversity within pericytes *Clin. Exp. Pharmacol. Physiol.* **27** 842–6

[36] Armulik A, Genové G and Betsholtz C 2011 Pericytes: developmental, physiological pathological perspectives, problems and promises *Dev. Cell* **21** 193–215

[37] Niland S and Eble J A 2012 Integrin-mediated cell-matrix interaction in physiological and pathological blood vessel formation *J. Oncol.* **2012** 1–25

[38] Galie P A, Nguyen D-H T, Choi C K, Cohen D M, Janmey P A and Chen C S 2014 Fluid shear stress threshold regulates angiogenic sprouting *Proc. Natl Acad. Sci. USA* **111** 7968–73

[39] Song H H G, Lammers A, Sundaram S, Rubio L, Chen A X, Li L, Eyckmans J, Bhatia S N and Chen C S 2020 Transient support from fibroblasts is sufficient to drive functional vascularization in engineered tissues *Adv. Funct. Mater.* **30** 2003777

[40] Sangwung P *et al* 2017 KLF2 and KLF4 control endothelial identity and vascular integrity *JCI Insight* **2** e91700

[41] Dekker R J, van Soest S, Fontijn R D, Salamanca S, de Groot P G, VanBavel E, Pannekoek H and Horrevoets A J G 2002 Prolonged fluid shear stress induces a distinct set of endothelial cell genes, most specifically lung Krüppel-like factor (KLF2) *Blood* **100** 1689–98

[42] Brisset A C, Isakson B E and Kwak B R 2009 Connexins in Vascular Physiology and Pathology *Antioxidants Redox Signaling* **11** 267–82

[43] Ranade S S *et al* 2014 Piezo1, a mechanically activated ion channel, is required for vascular development in mice *Proc. Natl Acad. Sci.* **111** 10347–52

[44] Sivarapatna A, Ghaedi M, Le A V, Mendez J J, Qyang Y and Niklason L E 2015 Arterial specification of endothelial cells derived from human induced pluripotent stem cells in a biomimetic flow bioreactor *Biomaterials* **53** 621–33

[45] Hamada K, Oike Y, Ito Y, Maekawa H, Miyata K, Shimomura T and Suda T 2003 Distinct roles of Ephrin-B2 forward and EphB4 reverse signaling in endothelial cells *Arterioscler. Thromb. Vasc. Biol.* **23** 190–7

[46] Verberk WCEP, Sandkler J F, van de Pol I, Urbina M, Wilson R, McKenzie D J and Leiva F P 2022 Draft version of paper data and code of manuscript: body mass and cell size shape the tolerance of fishes to low oxygen in a temperature-dependent manner Zenodo (https://doi.org/10.5281/zenodo.6123770)